Supporting Information

Two Anthracene-Based Ir(III) Complexes $[Ir(pbt)_2(aip)]Cl$ and $[Ir(pbt)_2(aipm)]Cl$: Relationship Between Substituent Group and Photo-Oxidation Activity as well as Photo-Oxidation-Induced Luminescence

Qin-Zhen Yuan,[a§] Qianwenhao Fan,[a§] Hang Lv,[a] Wen-Wen Chen,[a] Xue-Xiao Yang,[a] Deng-Ke Cao*[a] and Jing Wen*[b]

[a] State Key Laboratory of Coordination Chemistry, School of Chemistry and Chemical Engineering, Nanjing University, Nanjing 210093, P. R. China

[b] Hubei Key Laboratory of Plasma Chemistry and Advanced Materials, School of Materials Science and Engineering, Wuhan Institute of Technology, Wuhan 430205, P. R. China

Quantum Chemical Calculation

All the quantum chemical calculations were implemented by the density functional theory (DFT) with long-range M06-2Xexchange-correlation functional[S1] and 6-31G(d) basis set,[S2] TS geometrical optimizations were performed by using the Berny algorithm. All the methods are integrated in Gaussian 09 D.01 program.[S3]

The geometrical and electronic structures of ligands aip and aipm were calculated first (Figure S19). It was found that the dihedral angle α between the imidazole-phenanthroline moiety and the anthracene moiety in aipm (α=62°) is significantly bigger than that in aip (α=52°). In addition, the middle benzene rings in the anthracene moieties from ligands aip and aipm show small difference in Mulliken charge (-0.01 e in aip and -0.04 e in aipm). These differences are mainly due to the different substituent group R_1 between aip and aipm (R_1 = H in aip while R_1 = CH_3 in aipm).

Subsequently, the structures of the adsorption products of O_2@aip-P and O_2@aipm-P were optimized (Figure S20). Considering that the photo-oxidation

products of aip and aipm have the structures of endoperxide with bridging singlet oxygen ($^1O_2$) on the middle benzene ring of the anthracene moiety (a triplet sensitizer), flexible scanning optimizations were carried out by stretching O_2 away from the middle benzene ring of the anthracene moiety in either aip or aipm (0.1 Å for each step). The structures with maximal total energies along this stretching pathway could be picked out as initial structures. Finally, the transition state (TS) structures were optimized with the picked out initial structures. Figure S20 shows the two possible pathways for O_2 adsorbing on the middle benzene rings of the anthracene moieties from aip and aipm, in which R denotes reactant, P for product and TS for transition state. Side1 represents the adsorbed O_2 and the substituent R1 = H or CH_3 at the same side of anthracene moiety, and side2 represents the case at different side.

Intrinsic reaction coordinate (IRC) was proposed by Fukui in 1970 as a path of chemical reactions,[S4] with the mass-weighted steepest descent path on the potential energy surface (PES). The imaginary frequency and IRC were examined to confirm the TS structures. In calculation, the step size of IRC path is the default 0.1 bohr, and the total step numbers are 50 points. By this reverse simulation, the hardly confirmed reactants of O_2@aip-R and O_2@aipm-R could be reasonably found out. Based on the first structures of IRC, the reactants could be obtained by triplet state optimizations (Figure S20). As a consequence, the activation energies ($E_{TS\text{-}R} = E_{TS} - E_R$) could be figured out (Table S2). Subsequently, the reaction rate constant were calculated to further describe the influence of substituent groups R_1 = H and CH_3 of aip and aipm during the O_2 adsorption process. The reaction rate constant were calculated by using the Arrhenius approach (see the below equation S1. A: a constant for the frequency of particle collisions, E: the activation energy of the reaction, R: the universal gas constant, and T: the absolute temperature.). In the case of this adsorption process, A is regarded as the same values here for O_2@aip and O_2@aipm with R = 8.314 $J \cdot mol^{-1} \cdot K^{-1}$ and T = 300 K.

$$k = Ae^{-E/RT} \qquad \text{(Equation S1)}$$

Based on the energy analyses, the four possible reaction pathways are feasible (Figure S20). However, the chemical reaction kinetics determines the final reaction

rate. According to the Arrhenius approach (equation S1), the reaction rate constant of O_2@aip-side1 (k_1) is significantly higher than the corresponding reaction rate constants of @aipm-side1 (k_2), O_2@aip-side2 (k_3) and O_2@aipm-side2 (k_4), obtaining k_1/k_2 = 49.1, k_1/k_3 = 1.5×10^5 and k_1/k_4 =1.6×10^5. These ratios indicate that the side2 adsorption is hardly feasible. The calculation details are showed as follows.

The ratio of reaction rate constants (k_1/k_2):

$$\frac{k_1}{k_2} = e^{\frac{-E_1+E_2}{RT}} = e^{\frac{(-0.0574+0.0611)\text{Ha}}{8.314\text{J}\cdot\text{mol}^{-1}\cdot\text{K}^{-1}\times 300\text{K}}} \approx e^{3.894} = 49.1$$

The ratio of reaction rate constants (k_1/k_3):

$$\frac{k_1}{k_3} = e^{\frac{-E_1+E_3}{RT}} = e^{\frac{(-0.0574+0.0687)\text{Ha}}{8.314\text{J}\cdot\text{mol}^{-1}\cdot\text{K}^{-1}\times 300\text{K}}} \approx e^{11.895} = 1.5\times 10^5$$

The ratio of reaction rate constants (k_1/k_4):

$$\frac{k_1}{k_4} = e^{\frac{-E_1+E_4}{RT}} = e^{\frac{(-0.0574+0.0688)\text{Ha}}{8.314\text{J}\cdot\text{mol}^{-1}\cdot\text{K}^{-1}\times 300\text{K}}} \approx e^{12.000} = 1.6\times 10^5$$

References

(S1) Y. Zhao, D. G. Truhlar, The M06 suite of density functionals for main group thermochemistry, thermochemical kinetics, non-covalent interactions, excited states, and transition elements: two new functionals and systematic testing of four M06-class functionals and 12 other functional. *Theor. Chem. Acc.* **2008**, 120, 215-241.

(S2) G. A. Petersson and M. A. Al-Laham, A complete basis set model chemistry. II. Open-shell systems and the total energies of the first-row atoms. *J. Chem. Phys.*, **1991**, 94, 6081-90.

(S3) M. J. Frisch, G. W. Trucks, H. B. Schlegel, G. E. Scuseria, M. A. Robb, J. R. Cheeseman, G. Scalmani, V. Barone, B. Mennucci, G. A. Petersson, H. Nakatsuji, M. Caricato, X. Li, H. P. Hratchian, A. F. Izmaylov, J. Bloino, G. Zheng, J. L. Sonnenberg, M. Hada, M. Ehara, K. Toyota, R. Fukuda, J. Hasegawa, M. Ishida, T. Nakajima, Y. Honda, O. Kitao, H. Nakai, T. Vreven, J. A. Montgomery, Jr. J. E. Peralta, F. Ogliaro, M. Bearpark, J. J. Heyd, E. Brothers, K. N. Kudin, V. N. Staroverov, R. Kobayashi, J. Normand, K. Raghavachari, A. Rendell, J. C. Burant, S.

S. Iyengar, J. Tomasi, M. Cossi, N. Rega, J. M. Millam, M. Klene, J. E. Knox, J. B. Cross, V. Bakken, C. Adamo, J. Jaramillo, R. Gomperts, R. E. Stratmann, O. Yazyev, A. J. Austin, R. Cammi, C. Pomelli, J. W. Ochterski, R. L. Martin, K. Morokuma, V. G. Zakrzewski, G. A. Voth, P. Salvador, J. J. Dannenberg, S. Dapprich, A. D. Daniels, O. Farkas, J. B. Foresman, J. V. Ortiz, J. Cioslowski, D. J. Fox, Gaussian 09, Revision D.01; Gaussian, Inc.: Wallingford, CT, **2009**.

(S4) K. Fukui, The path of chemical-reactions – The IRC approach, *Acc. Chem. Res.*, 1981, **14**, 363-368.

Table S1 The UV absorption bands of compounds **1**, **2**, pbtH, aip and aipm in CH_2Cl_2 at room temperature.

Compound	λ_{abs} (nm)
1	257, 281, 291, 311, 324, 350, 368, 387 and a tail towards 470
2	256, 295, 311, 324, 351, 370, 389 and a tail towards 470
pbtH	a broad peak in range 263-340
aip	256, 280, 293, 350, 368, 388
aipm	256, 284, 350, 368, 388

Table S2 The calculated total energies of reactants, transition states, and products of O_2@aip and O_2@aipm with O_2 adsorbed at side1 and side2. Based on the total energies, the activation energies ($E_{TS-R} = E_{TS} - E_R$) and reaction energies ($E_{P-R} = E_P - E_R$) are also figured out and showed in this table. At the thermodynamic point of view, negative reaction energy E_{P-R} means that the reaction is feasible, however, the reaction rate mainly depends on the activation energy E_{TS-R}.

Energy (Hartree) / Molecules	Reactant (R)	Transition State (TS)	Product (P)	E_{TS-R}	E_{P-R}
O_2@aip-side1	-1407.3346	-1407.2773	-1407.3502	0.0574	-0.0155
O_2@aipm-side1	-1446.6253	-1446.5642	-1446.6363	0.0611	-0.0110
O_2@aip-side2	-1407.3337	-1407.2649	-1407.3390	0.0687	-0.0053
O_2@aipm-side2	-1446.6246	-1446.5558	-1446.6293	0.0688	-0.0047

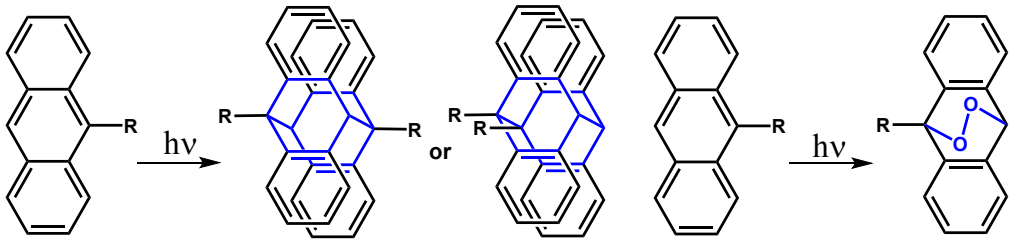

Scheme S1 The [4π + 4π] photodimerization reaction (left) and photo-oxidation reaction (right) for anthracene-based compounds.

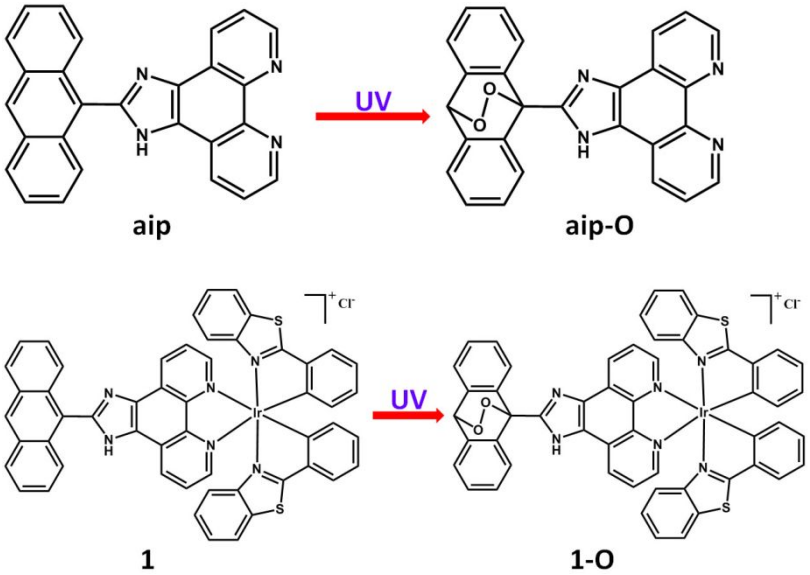

Scheme S2 The photo-oxidation behaviors of aip (top) and complex **1** (bottom).

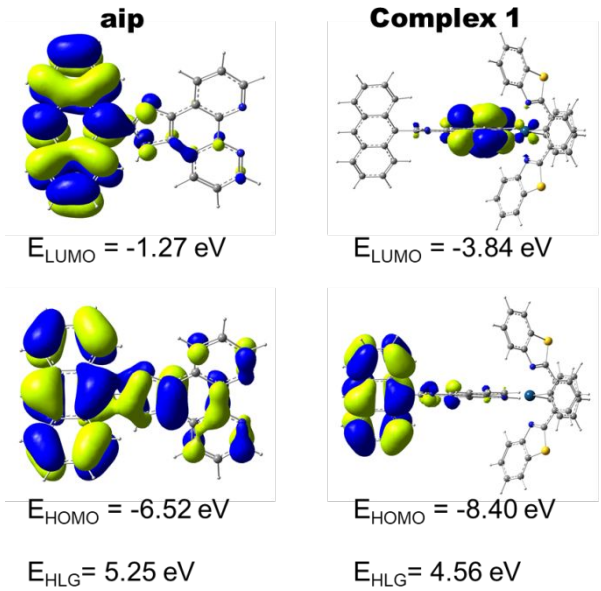

Scheme S3 The distributions and energy levels of the highest occupied and lowest unoccupied molecular orbitals (HOMO and LUMO) for free aip ligand and complex **1**.

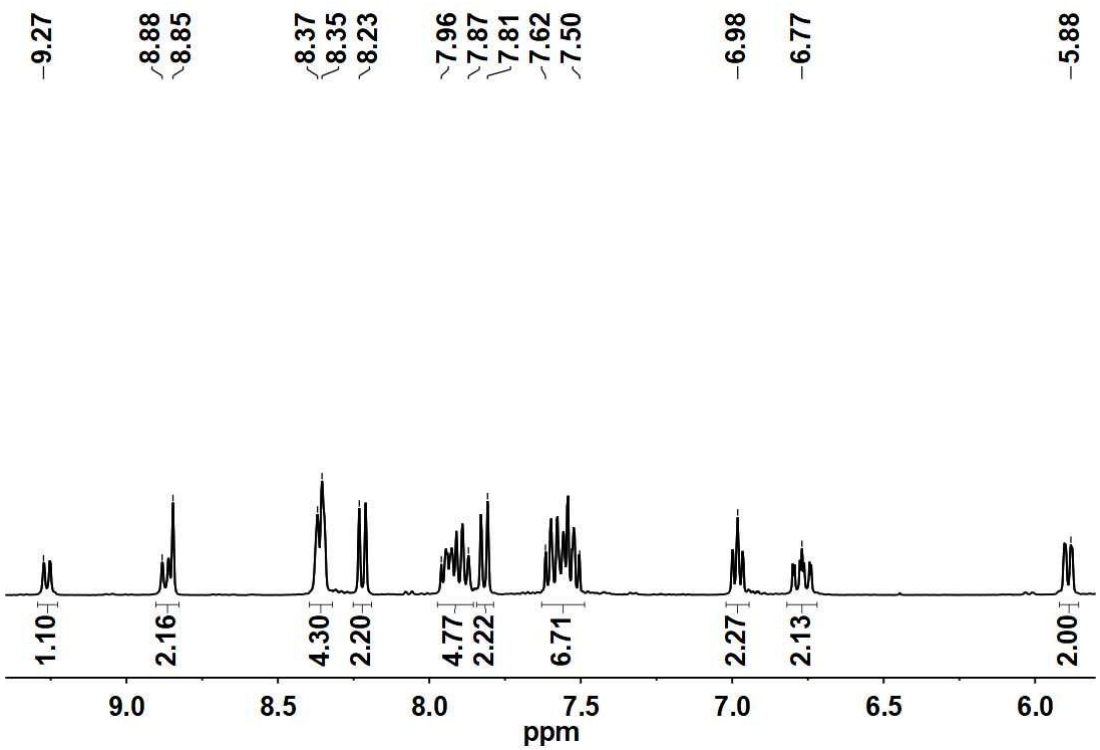

Figure S1. The ^{1}H NMR spectrum of complex $[Ir(dfppy)_2(aip)]PF_6$ (400 MHz, CD_3CN).

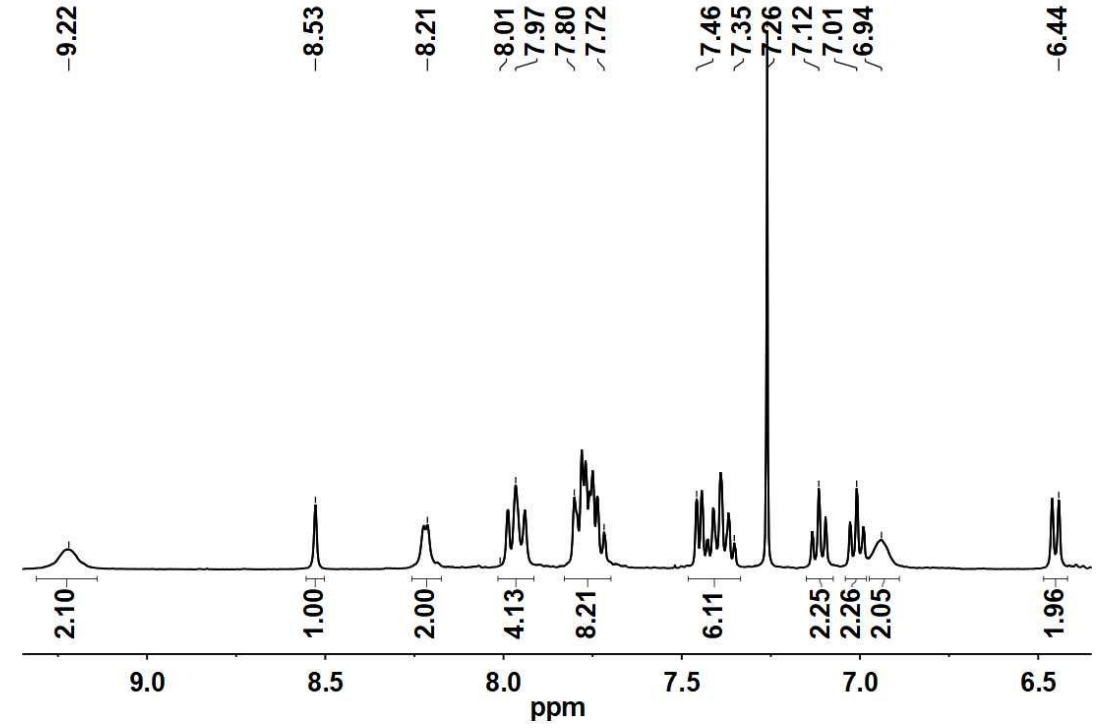

Figure S2. The ^{1}H NMR spectrum of complex $[Ir(ppy)_2(aip)]PF_6$ (400 MHz, $CDCl_3$).

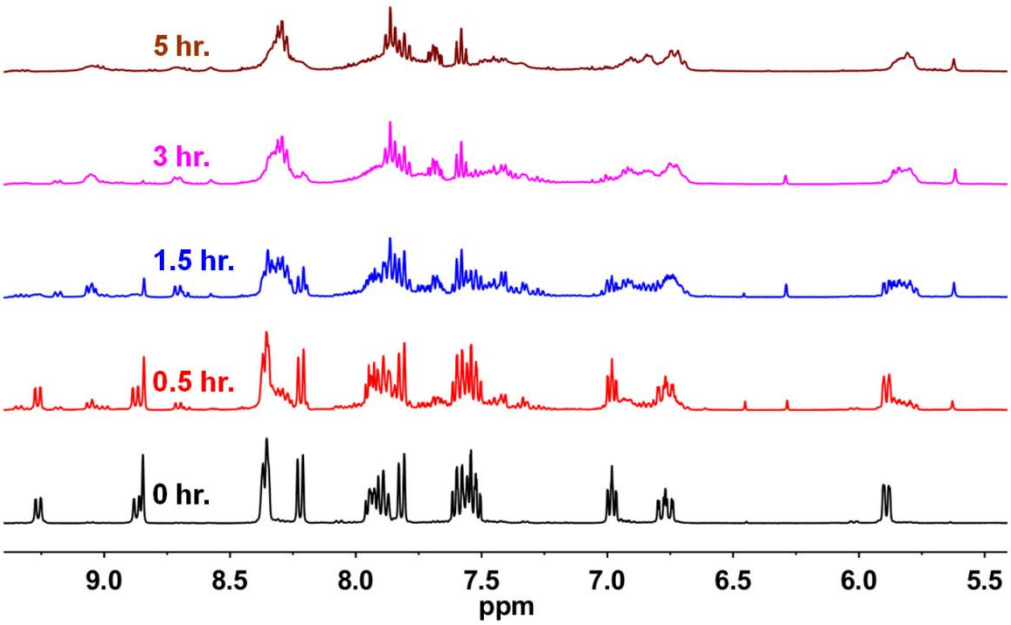

Figure S3. The ^{1}H NMR spectral changes of complex [Ir(dfppy)$_2$(aip)]PF$_6$ (400 MHz, CD_3CN) upon irradiation with 365 nm light.

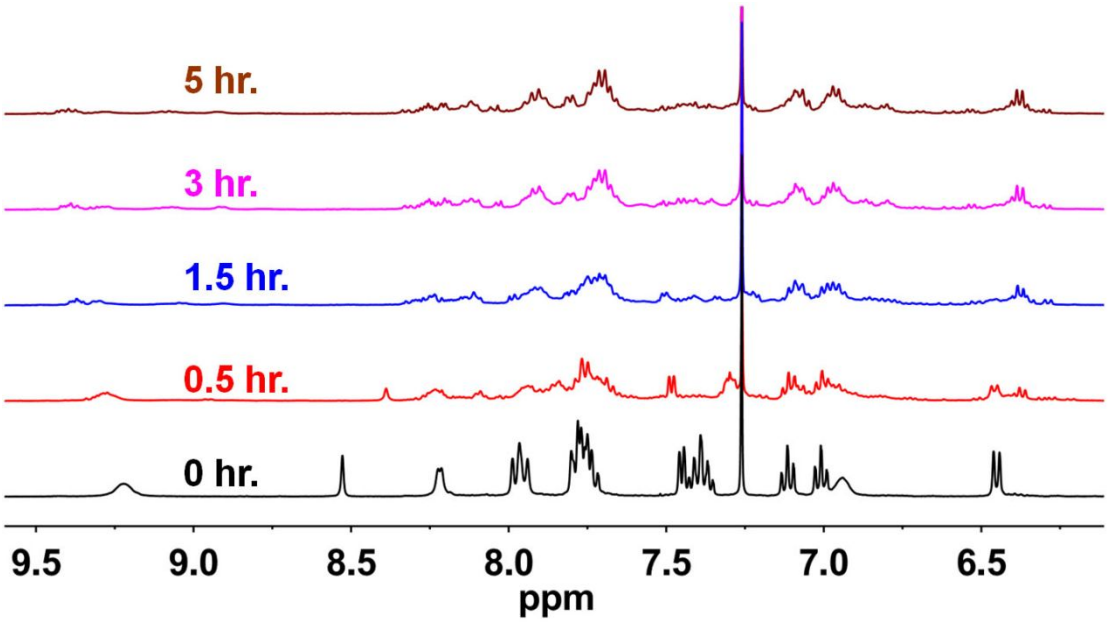

Figure S4. The ^{1}H NMR spectral changes of complex [Ir(ppy)$_2$(aip)]PF$_6$ (400 MHz, $CDCl_3$) upon irradiation with 365 nm light.

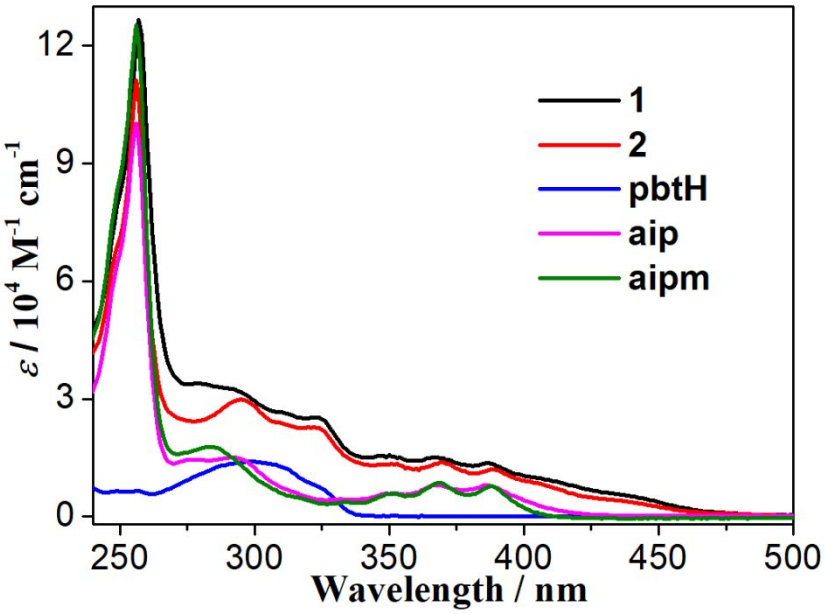

Figure S5. UV-vis absorption spectra of **1**, **2**, pbtH, aip and aipm in CH_2Cl_2 (c = 1 × 10^{-5} M).

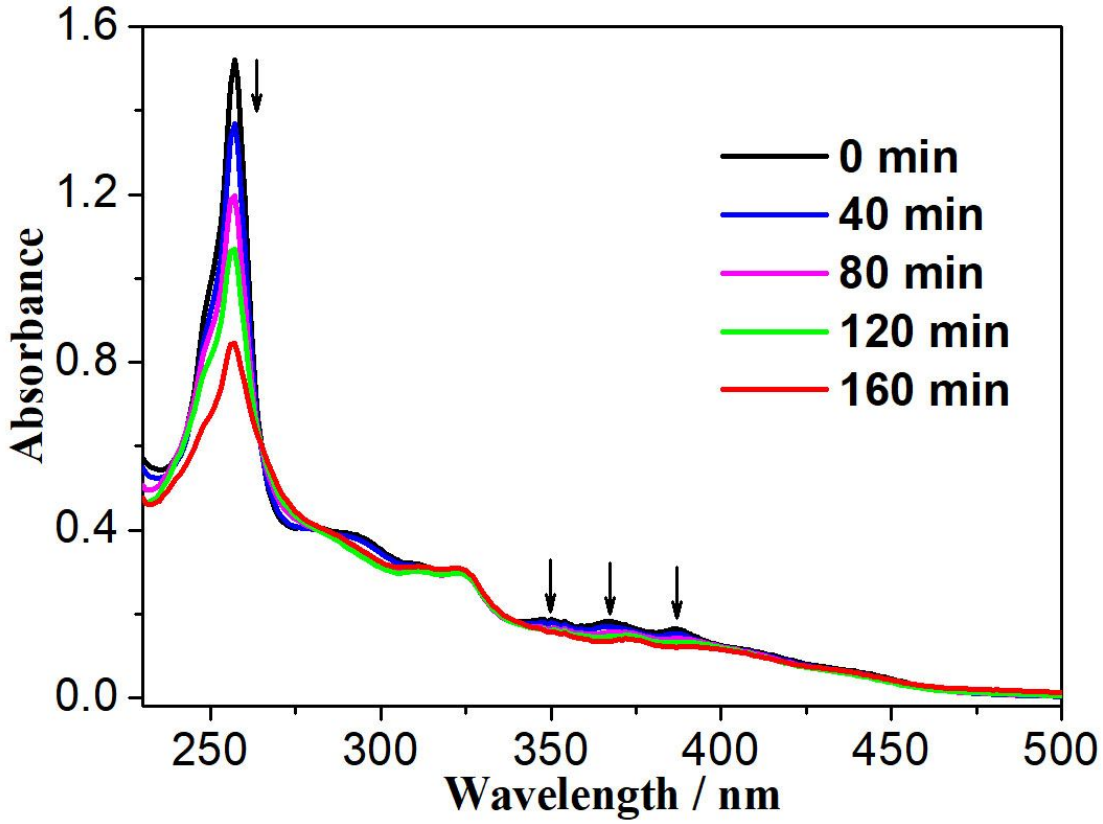

Figure S6. UV-vis absorption spectral changes of complex **1** in CH_2Cl_2 (c = 1 × 10^{-5} M) upon irradiation with 365 nm light.

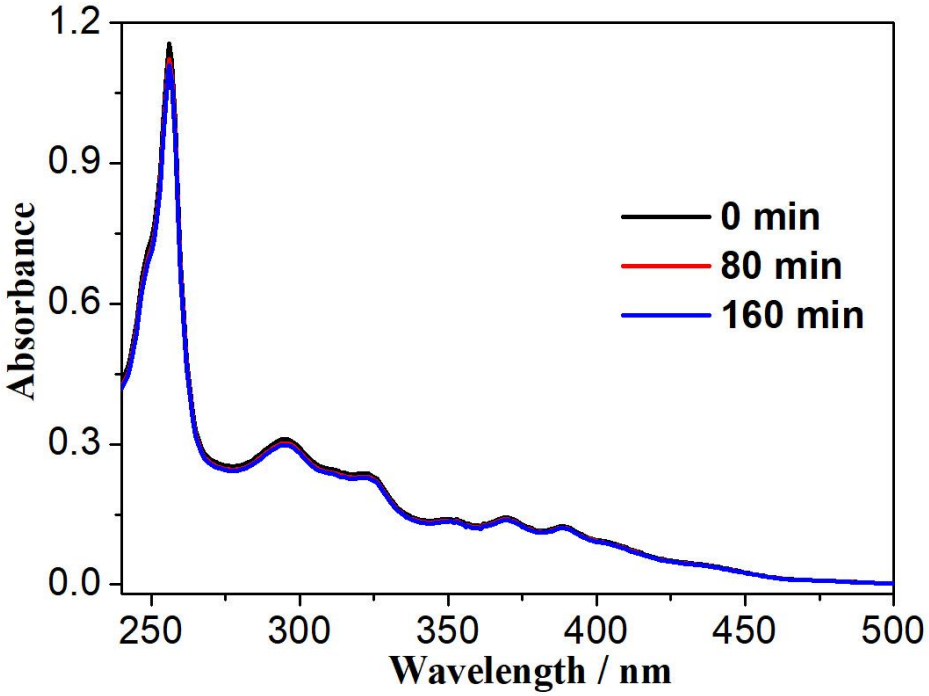

Figure S7. UV-vis absorption spectra of complex **2** in CH_2Cl_2 (c = 1 × 10^{-5} M) after irradiation with 365 nm light for different time.

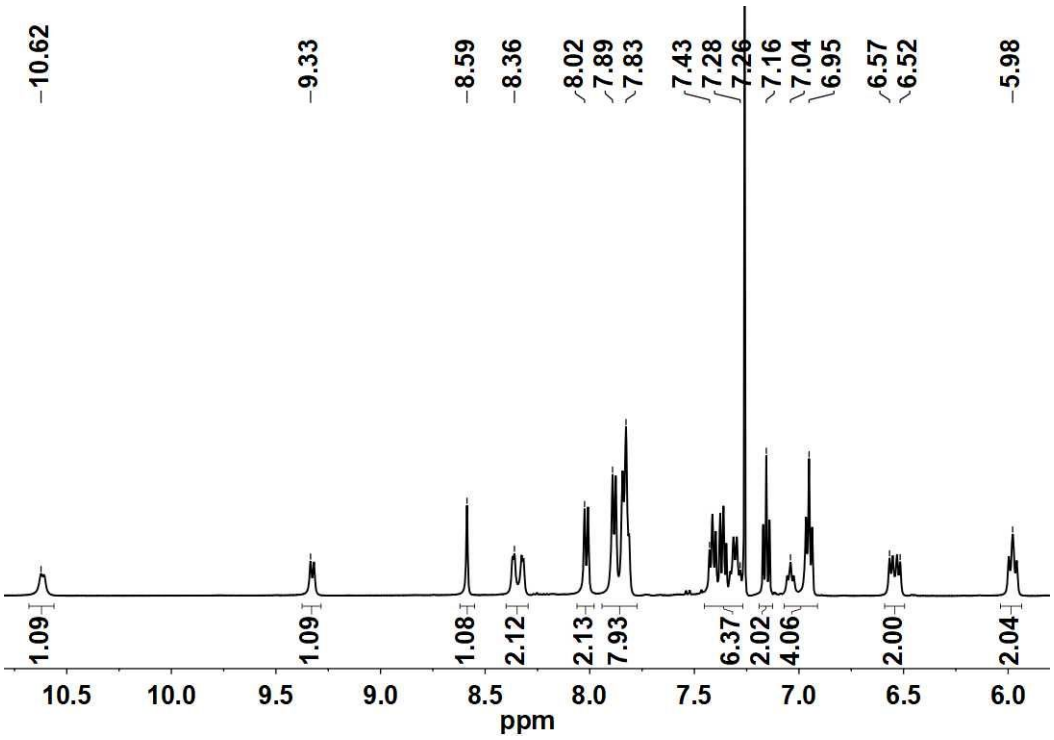

Figure S8. ^{1}H NMR spectrum of complex **1** (400 MHz, $CDCl_3$).

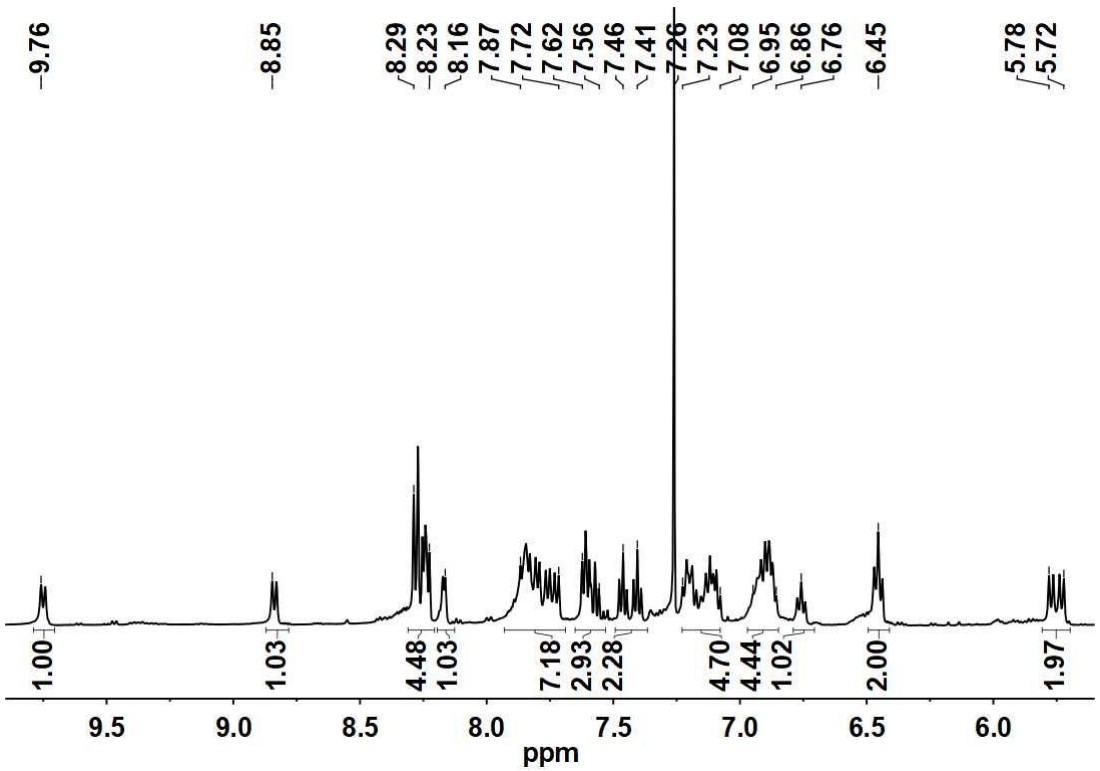

Figure S9. ^{1}H NMR spectrum of complex **1** (400 MHz, $CDCl_3$) after three-hour irradiation with 365 nm light, showing the peaks (ppm) at 5.72-5.78 (m, 2H), 6.45 (t, J = 4.4, 2H), 6.76 (t, J = 6.0 Hz, 1H), 6.86-6.95 (m, 4H), 7.08-7.23 (m, 4H), 7.41 (t, J = 6.0, 1H), 7.46 (t, J = 6.0, 1H), 7.56-7.62 (m, 3H), 7.72-7.87 (m, 6H), 8.16 (s, 1H), 8.23-8.29 (m, 4H), 8.85 (d, J = 3.2 Hz, 1H), and 9.76 (d, J = 3.2 Hz, 1H) [5.72-7.23 ppm and 7.41-9.76 ppm: total 31H from two pbt units and one aip ligand].

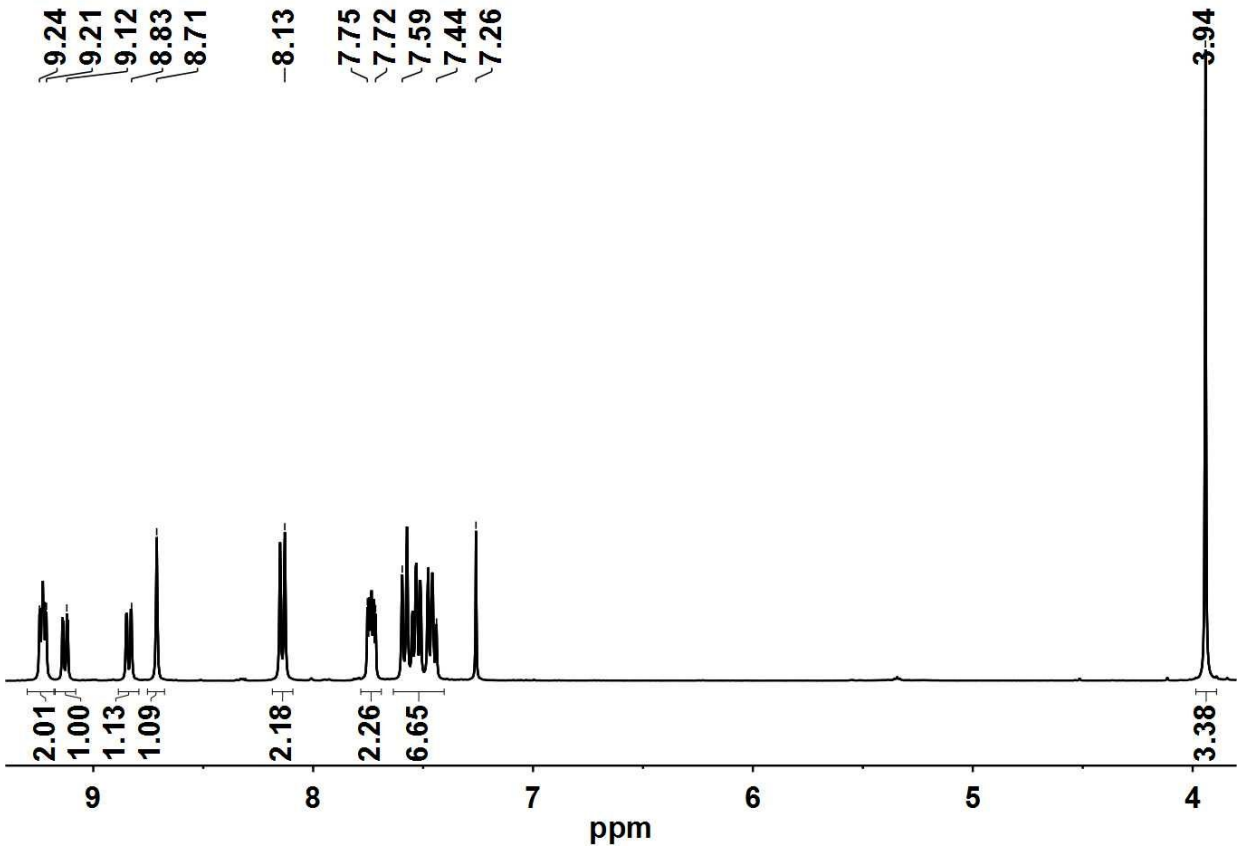

Figure S10. ^{1}H NMR spectrum of compound aipm (400 MHz, $CDCl_3$).

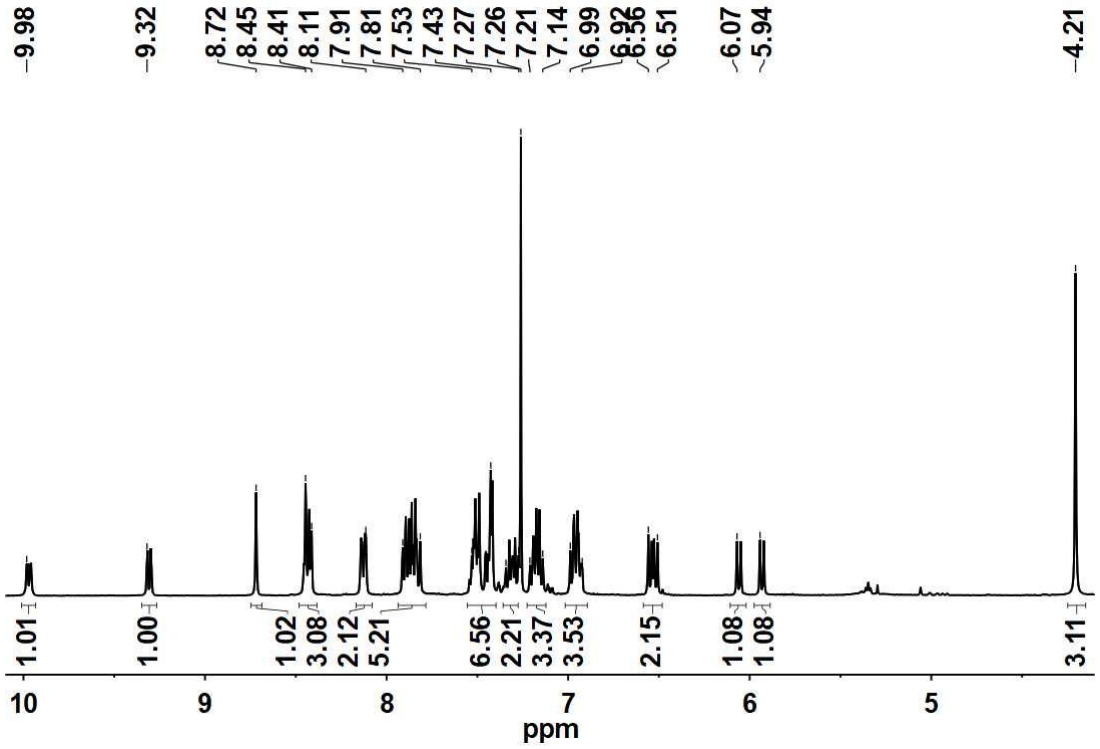

Figure S11. ^{1}H NMR spectrum of complex **2** (400 MHz, $CDCl_3$).

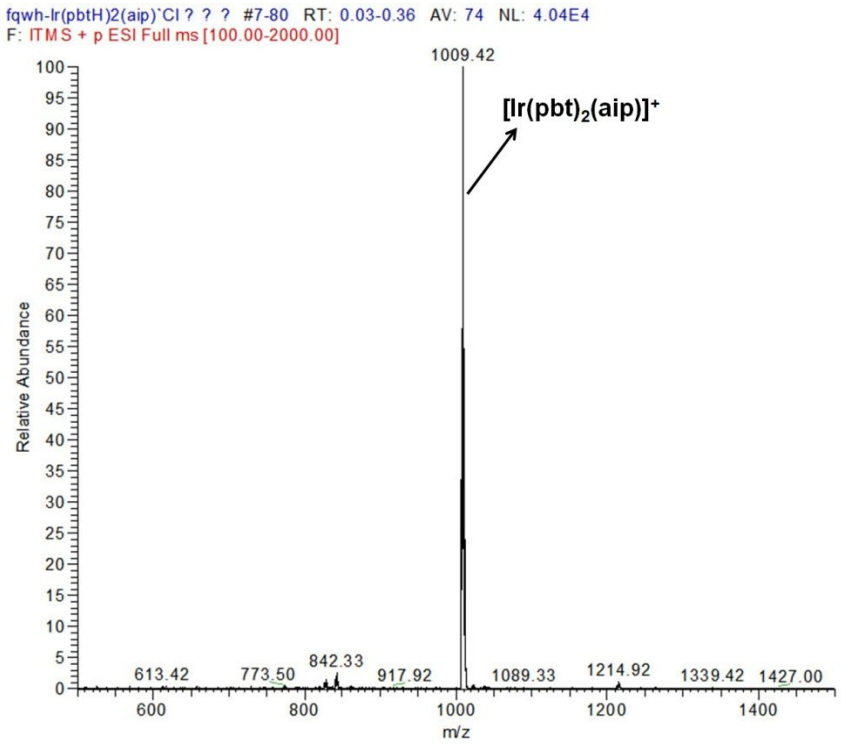

Figure S12. Electrospray (ES) mass spectrometry of **1** in CH_2Cl_2-CH_3OH solution.

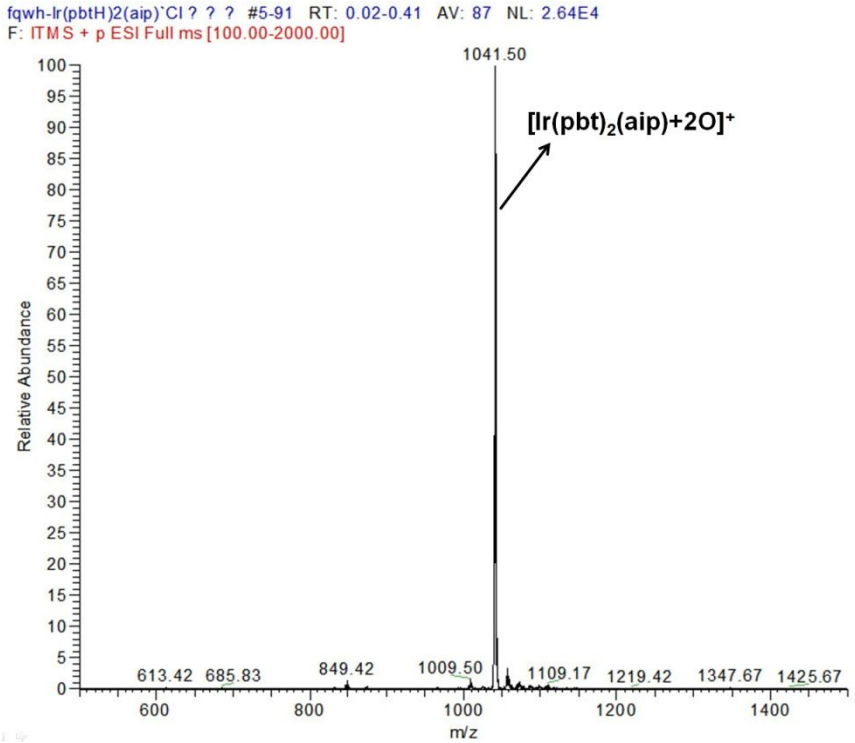

Figure S13. Electrospray (ES) mass spectrometry of complex **1** after undergoing photo-oxidation reaction in CH_2Cl_2.

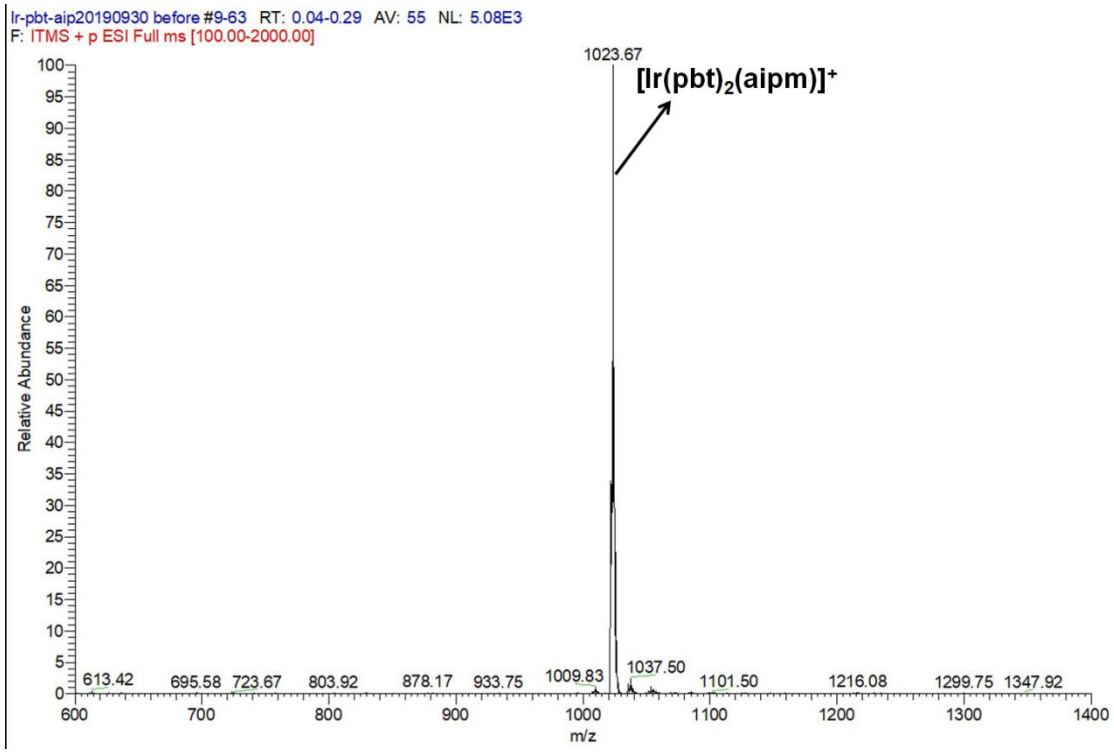

Figure S14. Electrospray (ES) mass spectrometry of **2** in CH_2Cl_2-CH_3OH solution.

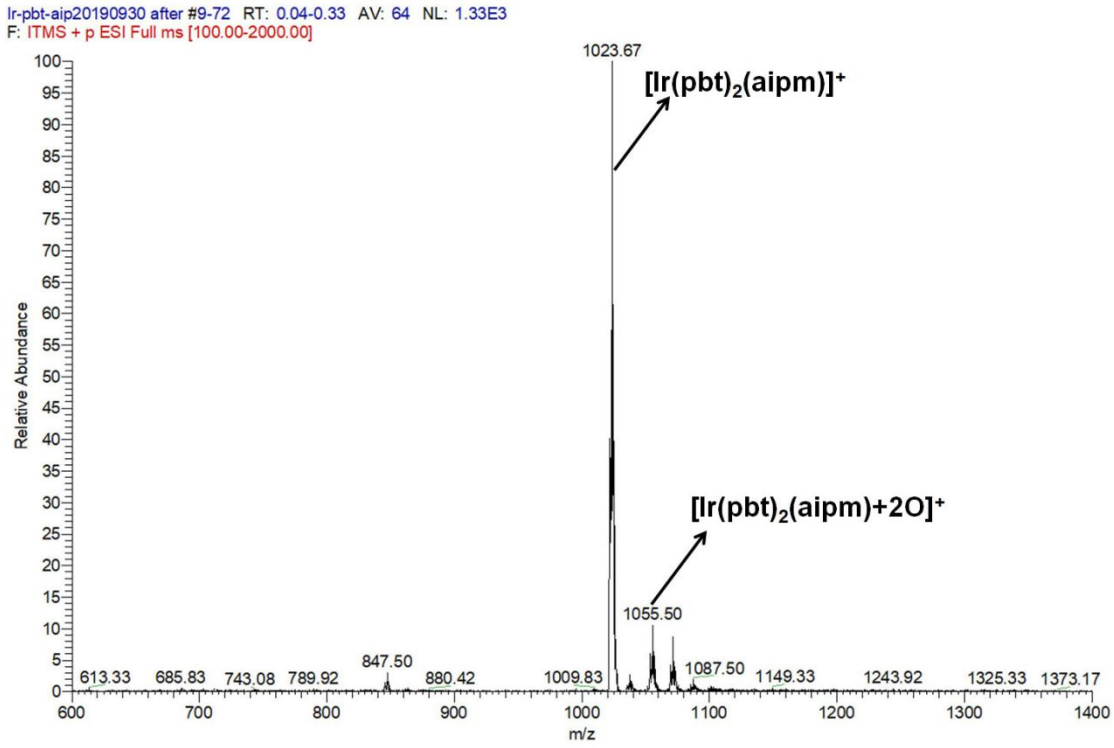

Figure S15. Electrospray (ES) mass spectrometry of **2** after five-hour irradiation with 365 nm light.

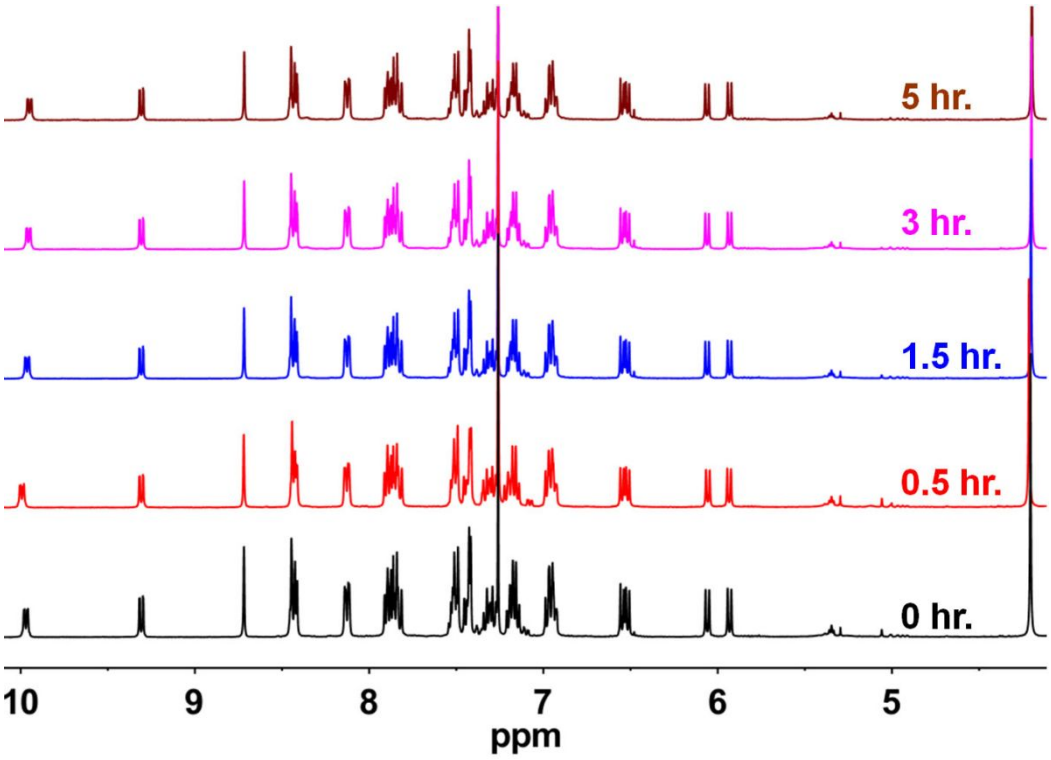

Figure S16. The ^{1}H NMR spectra of **2** (400 MHz, $CDCl_3$) after irradiation with 365 nm light for different time.

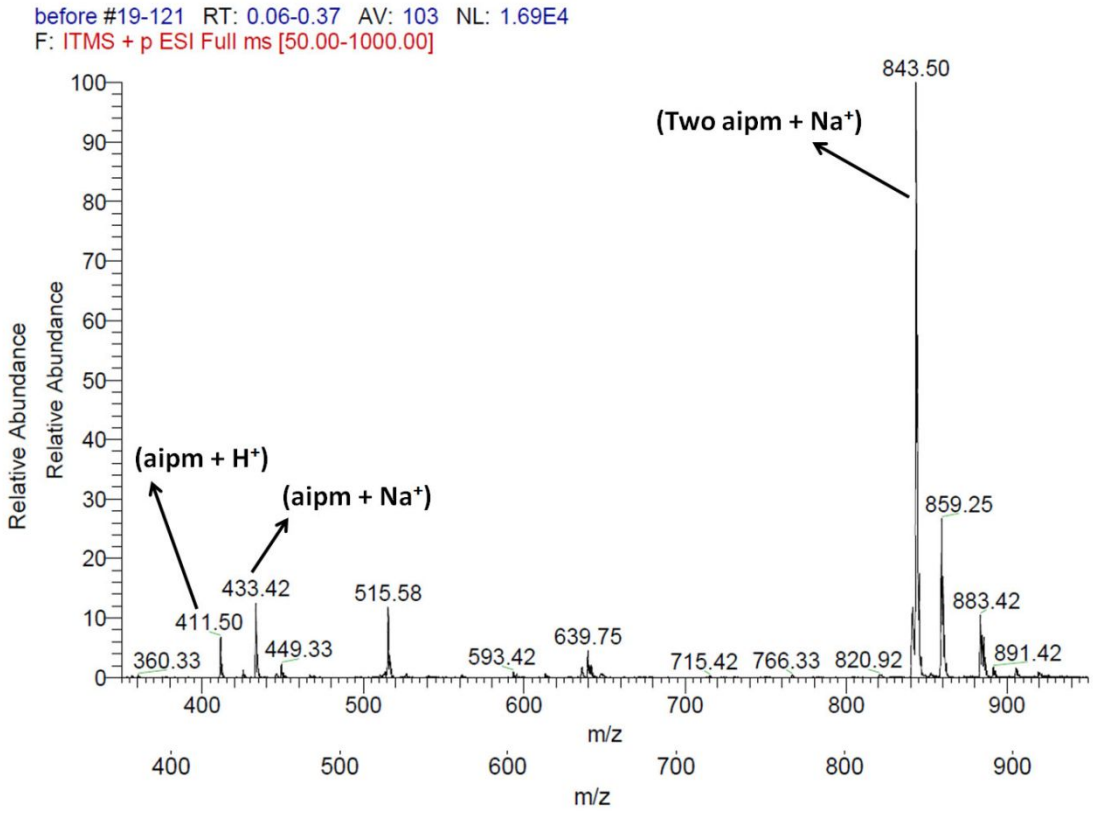

Figure S17. Electrospray (ES) mass spectrometry of aipm.

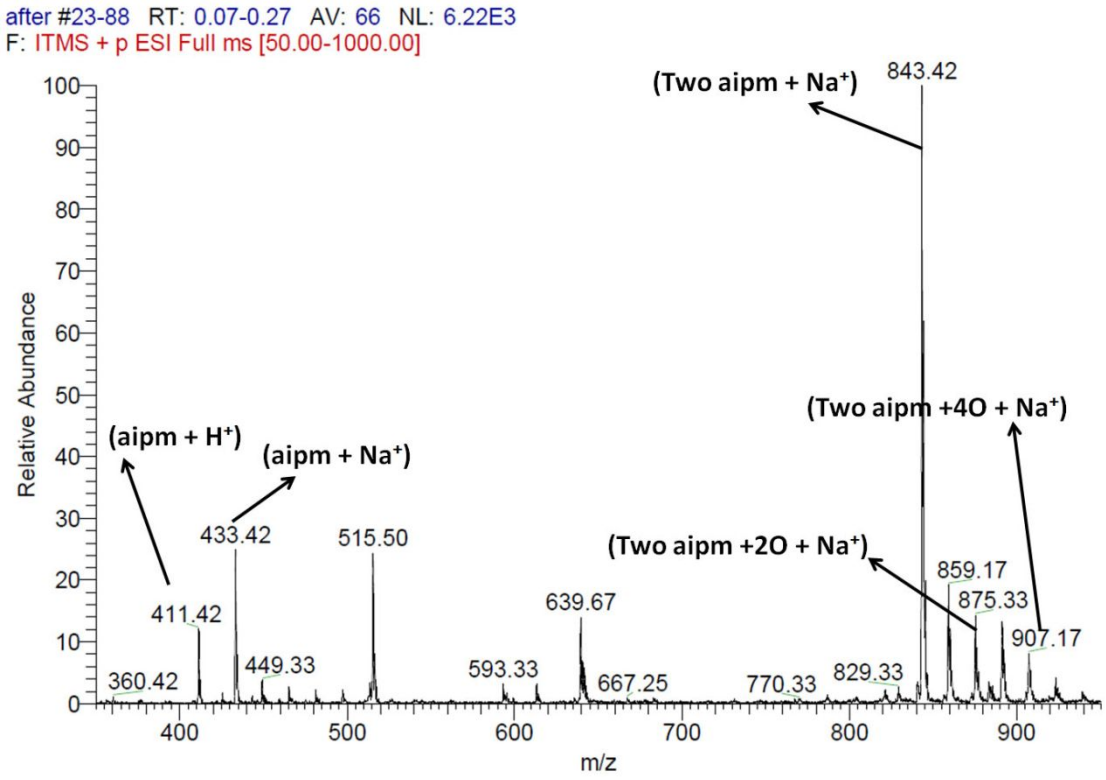

Figure S18. Electrospray (ES) mass spectrometry of aipm after irradiation with 365 nm light.

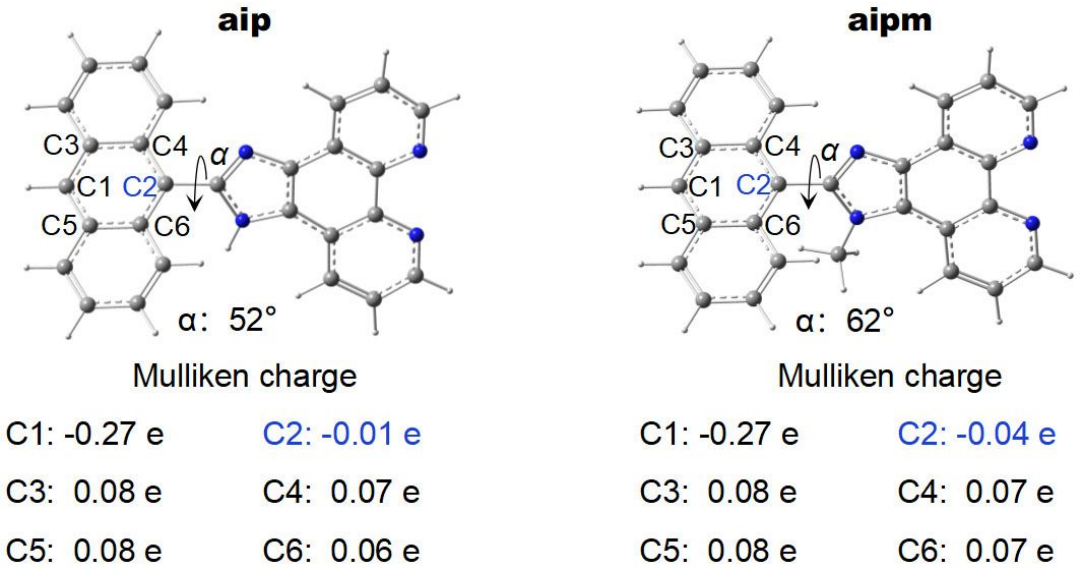

Figure S19. The optimized structures of aip and aipm, with the dihedral angle α between the imidazole-phenanthroline moiety and the anthracene moiety, and the Mulliken charge of the middle benzene ring in the anthracene moiety.

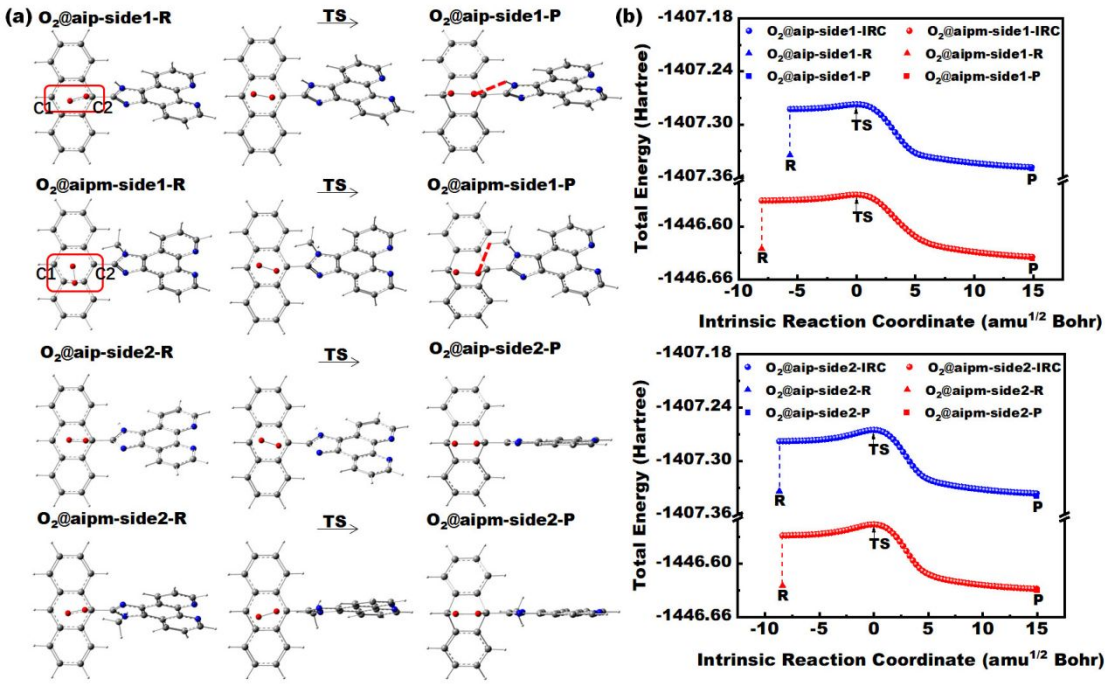

Figure S20. (a) Optimized structures of the reactants (R) and products (P) of O_2@aip and O_2@aipm adsorption models; (b) One of the possible intrinsic reaction coordinate pathway of the two adsorption models. The reactant and product are re-optimized to get their minimal total energies, and the transition state (TS) is the point when IRC equals 0.

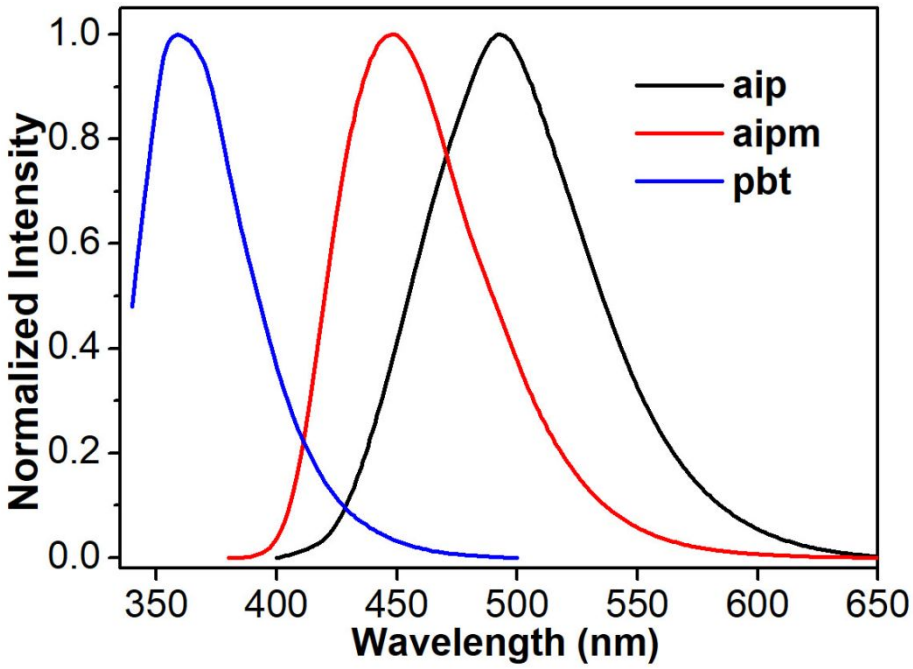

Figure S21 Luminescence spectra of compounds aip, aipm and pbtH in CH_2Cl_2 at room temperature.

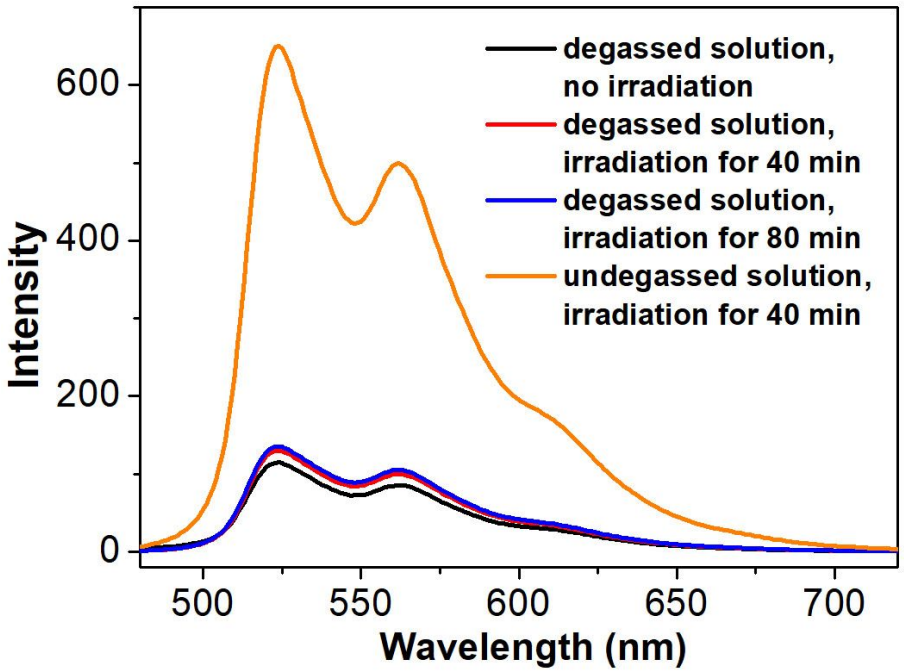

Figure S22 Luminescence spectral changes of **1** in CH_2Cl_2 upon irradiation with 365 nm light ($c = 1 \times 10^{-4}$ M, $\lambda_{ex} = 397$ nm).

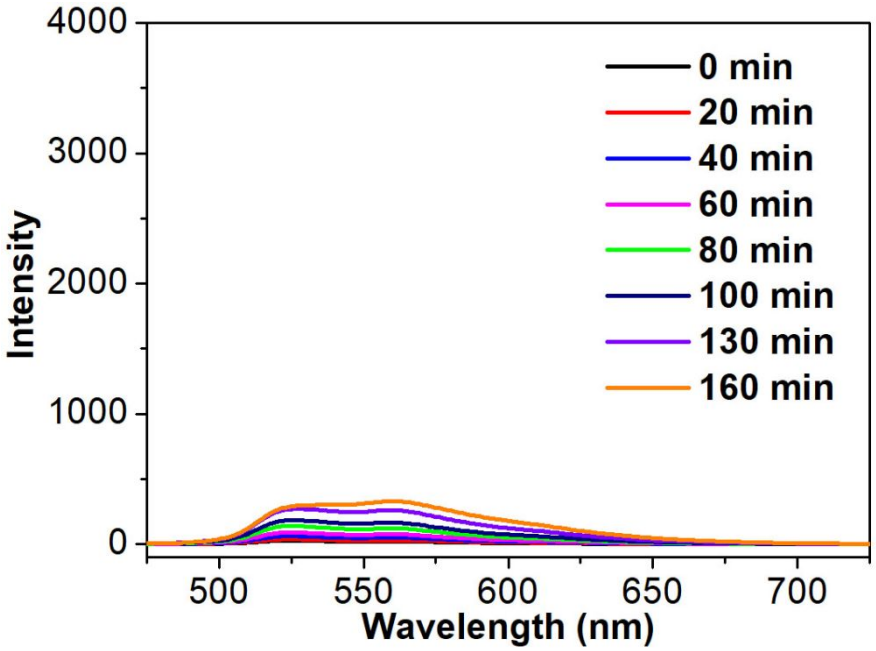

Figure S23 Luminescence spectral changes of **2** in CH_2Cl_2 upon irradiation with 365 nm light ($c = 1 \times 10^{-4}$ M, $\lambda_{ex} = 397$ nm).

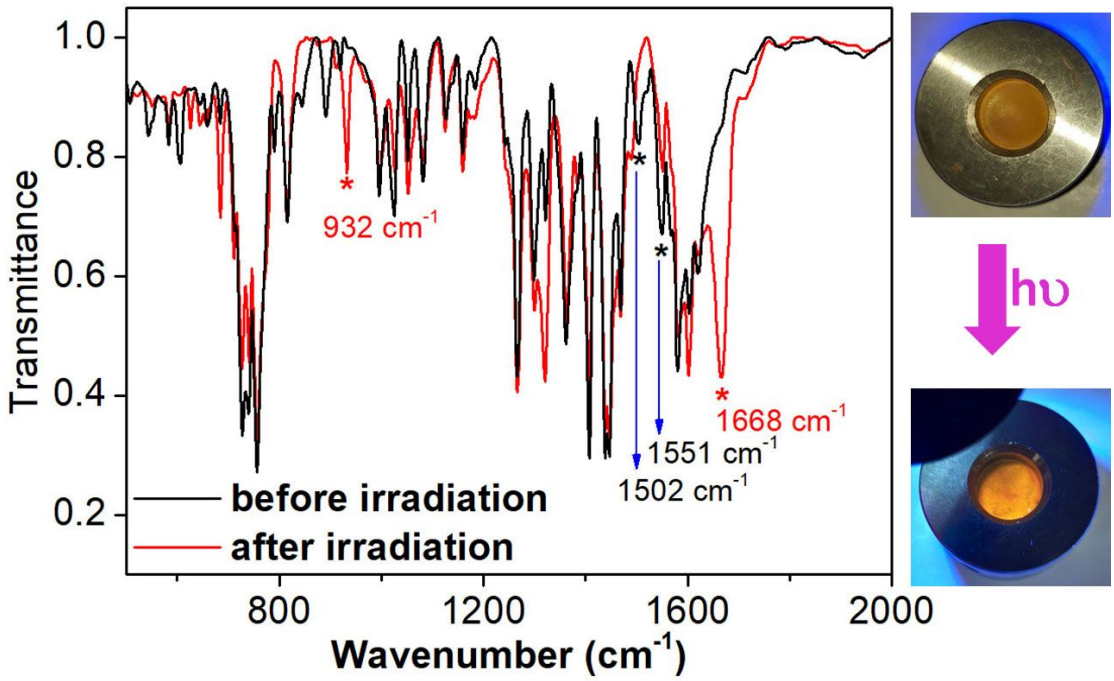

Figure S24 Left: IR spectra of complex **1** before and after irradiation with 365 nm light. Right: the luminescence photographs of KBr disk containing complex **1** before and after irradiation.